Supporting Information

Dual-molecule Reciprocal Doping Strategy for Cathode Interfacial Materials Enabling Over 20.7% Efficiency in Organic Solar Cells

Chengcheng Xie,[a] Yuanpeng Xie[a,*] Longjun Fu,[a] Xiaxia Yang,[a] Nian Zhang,[a] Bo Xu,[a] Zhuo Wang,[a] Dianyong Tang,[c] Liming Ding,[d] Feng Liu,[b,*] and Menglan Lv[a,*]

[a] Engineering Research Center for Energy Conversion and Storage Technology of Guizhou, School of Chemistry and Chemical Engineering, Guizhou University, Guiyang, P. R. China.
E-mail: mllv@gzu.edu.cn; ypxie@gzu.edu.cn

[b] Frontiers Science Center for Transformative Molecules, In-situ Center for Physical Science, and Center of Hydrogen Science, School of Chemistry and Chemical Engineering, Shanghai Jiao Tong University, Shanghai, P. R. China.
E-mail: fengliu82@sjtu.edu.cn

[c] Chongqing University of Arts and Sciences, Chongqing, P. R. China.

[d] School of Chemical Engineering and Light Industry, Guangdong University of Technology, Guangzhou, P. R. China.

Table of Contents

1. Synthesis Section

1.1 Materials

Amino-functionalized multi walled carbon nanotubes (CNT-N) were purchased from Suzhou Carbonrich Technology. All other chemicals and reagents were obtained from Sigma-Aldrich, Alfa Aesar, Aladdin, or other commercial suppliers, and were used as received without further purification.

1.2 Synthetic Details and Characterizations

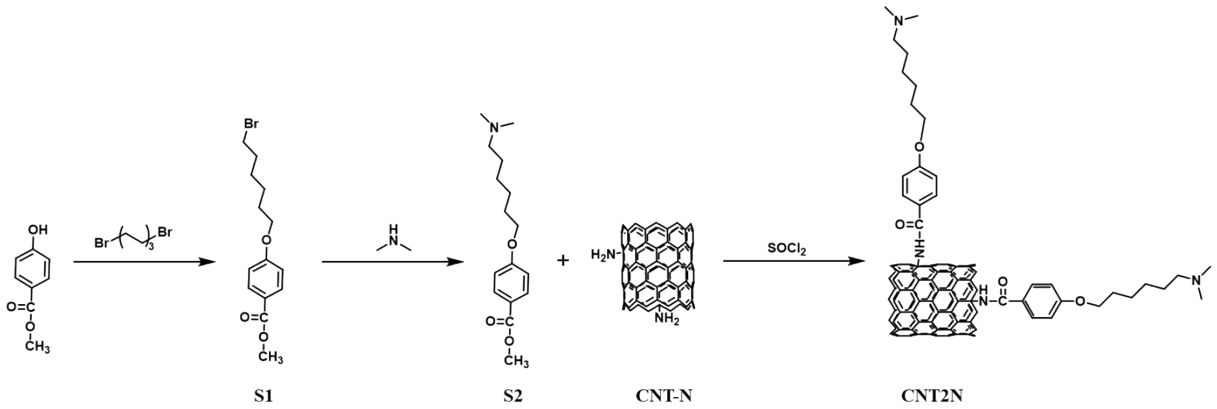

Figure S1. Synthetic route of CNT2N.

Synthesis of Compound S1. A mixture of Methyl 4-hydroxybenzoate (1.52 g, 10 mmol) and Cs_2CO_3 (4.8 g, 15 mmol) was dissolved in N,N-dimethylformamide under nitrogen atmosphere and stirred at 60 °C for 30 minutes. Subsequently, 1,6-dibromohexane (3.66 g, 50 mmol) was added dropwise, and the reaction was continued at 60 °C for 2 hours, with the progress monitored by thin-layer chromatography (TLC). Upon completion, the reaction mixture was extracted sequentially with ethyl acetate, water, and saturated brine. The organic phase was dried over anhydrous $MgSO_4$, filtered, and concentrated under reduced pressure to afford the crude product. The crude product was then purified by silica column chromatography using petroleum ether/ethyl acetate (10:1, v/v) as the eluent to yield the desired compound 1 as a white solid (2.71 g, yield: 86%). ^{1H} NMR (400 MHz, $CDCl_3$, δ): 7.97 (d, 1H), 7.95 (d, 1H), 6.89 (d, 1H), 6.87 (d, 1H), 3.99 (t, J = 6.4 Hz, 2H), 3.86 (s, 3H), 3.41 (t, J = 6.8 Hz, 2H), 1.88 (m, 2H), 1.79 (dd, J = 8.4, 5.2 Hz, 2H), 1.51-1.46 (m, 4H).

Synthesis of Compound S2. Compound 1 (0.32 g, 1 mmol) and potassium carbonate (0.42 g, 3 mmol) were dissolved in acetonitrile, followed by the slow addition of dimethylamine (0.092 g, 2 mmol). The amine was introduced dropwise to control its effective concentration and promote selective substitution at the bromoalkane site. Anhydrous acetonitrile was used as

the reaction solvent to facilitate the SN2 process while limiting undesired side reactions. The mixture was refluxed at 85 °C for 3 hours. The reaction progress was closely monitored by TLC and terminated immediately after completion. Upon completion of the reaction, the solvent was removed under reduced pressure. The residue was extracted sequentially with ethyl acetate, water, and saturated brine. The organic phase was dried over anhydrous $MgSO_4$, filtered, and concentrated under vacuum to afford the crude product. Purification by silica column chromatography using dichloromethane/methanol (7:1, v/v) as the eluent yielded the target compound S2 as a white solid (0.25 g, yield: 88%). ^{1H} NMR (400 MHz, $CDCl_3$, δ): 7.97 (d, J = 8.9 Hz, 2H), 6.88 (d, J = 9.0 Hz, 2H), 3.99 (t, J = 6.2 Hz, 2H), 3.87 (s, 3H), 2.87 (d, J = 18.7 Hz, 2H), 2.71 (s, 6H), 1.81 (d, J = 6.6 Hz, 2H), 1.44 (m, 4H), 1.27 (s, 2H), 1.23 (s, 2H).

General synthetic procedure of CNT2N. Based on an acyl chloride activation strategy, compound 2 was first subjected to acyl chloride activation. Specifically, compound S2 (0.2 g) was dissolved in dichloromethane, and thionyl chloride was added dropwise to the solution at room temperature. The mixture was stirred for 3 hours at room temperature, and excess thionyl chloride was subsequently removed under reduced pressure to yield the acyl chloride-activated intermediate of compound S2. CNT2N were synthesized according to published methods.[1] The resulting product was then mixed with CNT-N (20 mg) that had been pre-dispersed in DMF via ultrasonication. The reaction mixture was refluxed at 60 °C for 6 hours with continuous stirring. After completion, the solvent was removed, and the residue was washed twice with dichloromethane and methanol, respectively, and then dried for further use.

2. Experimental Section

2.1 Materials and measurements

Materials: The donor polymer PM6 and D18, the non-fullerene acceptors L8-BO and BTP-eC9 were purchased from Solarmer Materials Inc. The cathode interfacial materials PDINN, PNDIT-F3N were obtained from Nanjing Zhiyan Technology Co., Ltd. The hole-transporting material 2PAThCz was prepared as described in the literature.[2] Patterned high-transparency glass/ITO substrates with a sheet resistance of 15 Ω/sq were purchased from Youxuan Technology Co., Ltd.

General measurements: ^{1}H-NMR spectra of intermedia products and monomers were recorded at 400 MHz on a Bruker AVANCE spectrometer. Optical absorption spectra were recorded on a HITACHI U-2910 spectrometer with a slit width of 2.0 nm and a scan speed of 800 nm/min. Thermogravimetric analysis (TGA) data were obtained from a Pyris6

(PerkinElmer). X-ray photoelectron spectroscopy (XPS) analysis was performed using a Thermo Scientific K-Alpha photoelectron spectrometer. X-Ray Diffraction (XRD) patterns were analyzed employing a Rigaku SmartLab SE diffractometer, utilizing Cu Kα1 irradiation. Fourier Transform Infrared (FT-IR) measurements were performed using a Thermo Scientific Nicolet iS 10, and Raman spectra were recorded using an alpha300 R-WITec Raman spectrometer equipped with a 473 nm blue laser as the excitation source. Transmission electron microscopy (TEM) images were acquired using a JEOL JEM-F200 instrument. Atomic Force Microscope (AFM) images were recorded using a Digital Instruments Nanoscope IIIa multimode atomic force microscope in tapping mode under ambient conditions. Photoluminescence Spectroscopy (PL) measurements were performed with an excitation wavelength of 450 nm and measured over the range of 500 to 850 nm with steps of 5 nm.

2.2 Fabrication and characterization

Preparation of CNT- or CNT2N-doped PDINN solution: Following a previously reported procedure,[3,4] PDINN was doped using an ultrasound-assisted method to prepare mixed solutions of PDINN-CNT2N and PDINN-CNT. Briefly, a specified amount of CNT2N or CNT was dispersed in methanol at a concentration of 0.5 mg/mL and ultrasonicated (Dongsen DS-040ST) in an ice-water bath for 2 hours to obtain a uniformly dispersed methanol solution of CNT2N or CNT. The resulting dispersion was then added to a pre-prepared PDINN solution at various weight ratios (3%, 5%, 7%, 10% and 15%) relative to PDINN. The final PDINN concentration in the mixed solution was adjusted to 1 mg/mL. The mixture was further ultrasonicated in an ice-water bath for 1 hour to yield the PDINN-CNT2N or PDINN-CNT composite interfacial layer solution.

Solar cells: Patterned glass/ITO substrates were sequentially ultrasonicated for 15 minutes each in detergent solution, deionized water, acetone, and isopropanol. The cleaned substrates were then treated with oxygen plasma for 10 minutes. A methanol solution of 2PAThCz (0.3 mg/mL) was subsequently spin-coated onto the ITO surface, followed by thermal annealing at 100 °C for 5 minutes. The substrates were then transferred into a nitrogen-filled glovebox. A chloroform solution of PM6:L8-BO (15 mg/mL, weight ratio 1:1.2) containing 13 mg/mL of 1,3-dibromo-5-chlorobenzene as an additive was spin-coated onto the 2PAThCz-modified surface at 3000 rpm to form an ~90 nm-thick photoactive layer, followed by thermal annealing at 80 °C for 7 minutes. For the D18:L8-BO (1:1.2, w/w) and D18:L8-BO:BTP-eC9 (1:0.7:0.5, w/w/w) systems, chloroform solutions with a polymer concentration of 6 mg/mL and 1,4-diiodobenzene (6 mg/mL) as the additive were spin-coated at 3000 rpm onto the 2PAThCz

surface at 90 °C, followed by annealing at 100 °C for 5 minutes. Subsequently, the prepared PDINN-CNT2N solution was spin-coated at 3000 rpm onto each type of active layer. Finally, silver electrodes (120 nm) were thermally evaporated under high vacuum to complete the device fabrication. Devices based on PDINN-CNT and pristine PDINN CIMs were fabricated under the same conditions for comparison.

***J-V* and EQE characterization:** The current density-voltage (*J-V*) characteristics were measured inside a nitrogen-filled glovebox under AM 1.5G illumination (100 mW cm^{-2}) provided by a solar simulator (Enlitech model SS-X50). The light intensity was calibrated using a standard silicon reference cell equipped with a KG5 filter, certified by the National Institute of Metrology. Measurements were carried out using a Keithley 2400 source meter. The active device area was defined as 0.0312 cm^2 using a shadow mask. External quantum efficiency (EQE) spectra were measured using a solar cell spectral response measurement system (QE-R3011, Enli Technology Co., Ltd). Film thicknesses were determined using a surface profilometer (Dektak XT, Bruker).

2.3 Density Functional Theory Calculations

To investigate the interaction between PDINN and CNT2N, a carbon nanotube with a diameter of 15 nm was constructed through computational modeling. Periodic density functional theory (DFT) calculations and geometry optimizations were performed using the CP2K simulation package, which incorporates Troullier–Martins norm-conserving pseudopotentials and numerical localized basis sets. The orbital-confining cutoff was determined by an energy shift of 0.010 eV. All atoms were described using an optimized double-ζ plus polarization (DZP) basis set. The exchange-correlation interactions were treated using the generalized gradient approximation (GGA) with the Perdew-Burke-Ernzerhof (PBE) functional and Γ-point sampling. Owing to the large molecular size, dispersion interactions were included using the D3BJ correction scheme. Geometry relaxation was carried out using the quasi-Newton L-BFGS method until the maximum force on each relaxed atom was below 0.05 eV/Å. Subsequently, the most stable structure obtained from SIESTA was further optimized using the Vienna Ab initio Simulation Package (VASP). The projector-augmented wave method was employed to describe the interaction between core and valence electrons. The PBE functional was used to account for electron exchange and correlation effects. A Gaussian smearing of 0.1 eV was applied to enhance the convergence of states near the Fermi level. The plane-wave energy cutoff was set to 400 eV, and Brillouin zone sampling was restricted to the Γ point. Van der Waals interactions were considered by incorporating pairwise

atomic terms using the DFT-D3 method with Becke–Johnson damping to correct the Kohn-Sham DFT energy. The convergence criteria for electronic and geometric structures were set to 10^{-4} eV and 0.05 eV·Å^{-1}, respectively.

2.4 GIWAXS measurement

Grazing-incidence wide-angle X-ray scattering (GIWAXS) measurements were conducted at the Diffuse X-ray Scattering Beamline (1W1A) of the Beijing Synchrotron Radiation Facility (BSRF). Thin-film samples were prepared on silicon (Si) substrates using blend solutions identical to those used in device fabrication. The measurements were conducted at an incidence angle ranging from 0.1° to 0.2°. The coherence length was calculated using the Scherrer equation: CCL = 2πK/Δq, where Δq is the full width at half maximum (FWHM) of the diffraction peak in reciprocal space, and K is the shape factor (a value of 0.90 was used in this study).

2.5 Ultraviolet Photoelectron Spectrometer Measurements

Ultraviolet photoelectron spectroscopy (UPS) measurements were conducted using a Kratos Supra spectrometer equipped with a helium discharge lamp (He I line, 21.22 eV) as the ultraviolet excitation source. The work function (E_F) was calculated using the equation: E_F = 21.22 eV - E_{cutoff}. To compensate for the instrument work function and to exclude low kinetic energy electrons, a -5 V bias was applied to all samples, and the energy scale of the experimental data was adjusted by 5 eV accordingly.

2.6 Conductivity measurements

The *I-V* characteristics was measured by a Keithley 2400 source meter with the device structure of ITO/CIMs/Ag based on Ohm's law. The precleaned ITO substrates were treated with plasma for 10 minutes. Then, the 40 nm CIM was spin-coated on the ITO substrates. About 120 nm Ag was thermally evaporated under high vacuum. The *I-V* characteristics of these devices were measured in the dark. The conductivity was calculated using the equation of σ = IL/US, where L is the thickness of the CIMs and S is the device area. Note that the thickness of the three CIMs should be the equal.

2.7 Space-charge-limited current (SCLC) measurements

The space-charge-limited current (SCLC) measurements were conducted on electron-only devices with the architecture ITO/ZnO/PM6:L8-BO/CIMs/Ag. The preparation of the CIMs

and the PM6:L8-BO active layer followed the same procedures used for OSC fabrication. The electron mobility was extracted from the *J-V* curves and calculated using the Mott-Gurney equation:

$$J = \frac{9}{8}\varepsilon_0\varepsilon_r\mu\frac{V^2}{d^3}$$

where J is the current density, ε_0 is the vacuum permittivity, ε_r is the relative dielectric constant of the blend film (assumed to be 3.0), μ is the charge carrier mobility, V is the effective applied voltage, and d is the thickness of the film.

2.8 Device stability

The devices were encapsulated and placed in a testing chamber under ambient air conditions. *J-V* curves were recorded at 10 minutes intervals under continuous LED illumination. The light intensity was calibrated using a standard silicon reference cell.

2.9 Electrochemical impedance spectroscopy (EIS) measurements

Electrochemical Spectroscopy impedance spectroscopy (ElS) measurements were conducted using a Interface 1010E electrochemical workstation. The measurements were executedin a dark environment, applying a bias equal to the open circuit voltage. The frequency range spanned from 10^5 Hz to 0.1 Hz, with an AC potential amplitude of 100 mV.

2.10 Mott-Schottky curves

Mott-Schottky analysis of the OSCs was carried out over a DC bias range of 0.1-1 V under dark conditions, using an AC modulation frequency of 5000 Hz. The amplitude of the AC potential was set to 5 mV.

2.11 Light Intensity dependence measurements

The dependencies of open-circuit voltage (V_{oc}) and short-circuit current density (J_{sc}) on light intensity were measured under AM 1.5G illumination in a nitrogen-filled glovebox, with light intensity varied continuously from 10 to 100 mW cm^{-2}. These measurements were performed using a Keithley 2400 source meter and a calibrated reference silicon solar cell equipped with a KG5 filter. The effective device area was defined as 0.0312 cm^2 using a shadow mask. Typically, the data are fitted using the equation $V_{oc} \propto nkT/q \ln(P_{light})$, where q, T, and k represent the elementary charge, absolute temperature in Kelvin, and Boltzmann constant, respectively.[5] The ideality factor n, extracted from the slope of the fitted line, generally falls within the range of 1 to 2, indicating the presence of charge carrier traps either within the active

layer or at the interfaces. The dependence of J_{sc} on light intensity (P_{light}) reflects the extent of bimolecular recombination, characterized by the exponential factor α in the relationship $J_{sc} \propto P_{light}^{\alpha}$. An α value closer to 1 indicates that nearly all photogenerated charge carriers are efficiently collected by the electrodes.[6,7]

2.12 Photocurrent density versus effective voltage measurements

The relationship between the photocurrent density (J_{ph}) and the effective voltage (V_{eff}) of the device was determined from the current density-voltage (*J-V*) characteristics measured under both illuminated and dark conditions, using a voltage scan range from -2 to 2 V. The photocurrent density was defined as $J_{ph} = J_L - J_D$, where J_L and J_D represent the current densities under AM 1.5G illumination (100 mW cm^{-2}) and in the dark, respectively. The effective voltage was calculated as $V_{eff} = V_0 - V_{appl}$, where V_0 is the voltage at which $J_{ph} = 0$, and V_{appl} is the applied voltage. At sufficiently high V_{eff}, all free charge carriers in the active layer are efficiently extracted by the electrodes, which are assumed to be temperature-independent under these conditions. When V_{eff} reaches 2 V, complete exciton dissociation is assumed, leading to the saturated photocurrent density (J_{sat}). Exciton dissociation efficiency (P_{diss}) and charge collection efficiency (P_{coll}) can then be quantitatively evaluated based on this condition.[8]

3. Supplementary Figures

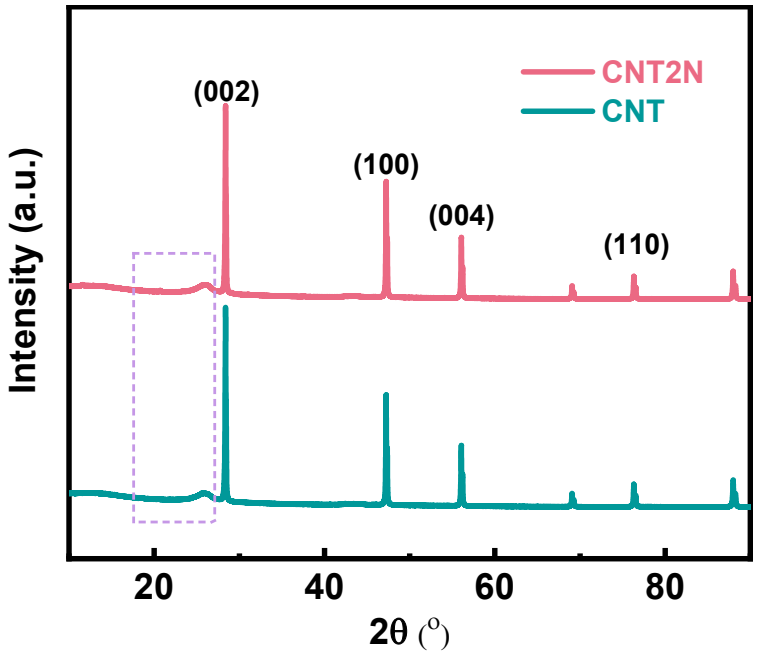

Figure S2. XRD patterns of CNT2N and CNT.

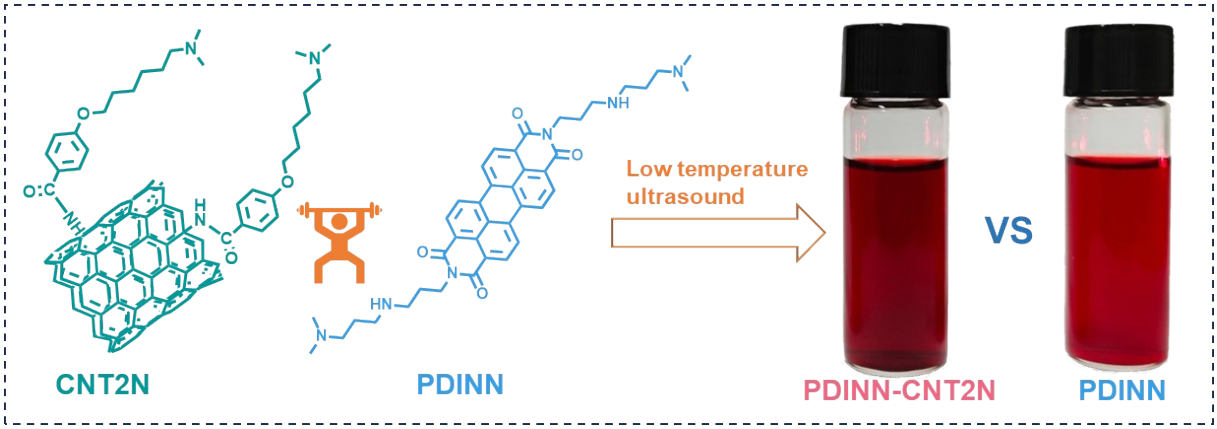

Figure S3. Schematic illustration of PDINN-CNT2N hybrid CIM preparation. (1 mg mL^{-1} PDINN with 7 wt% CNT2N).

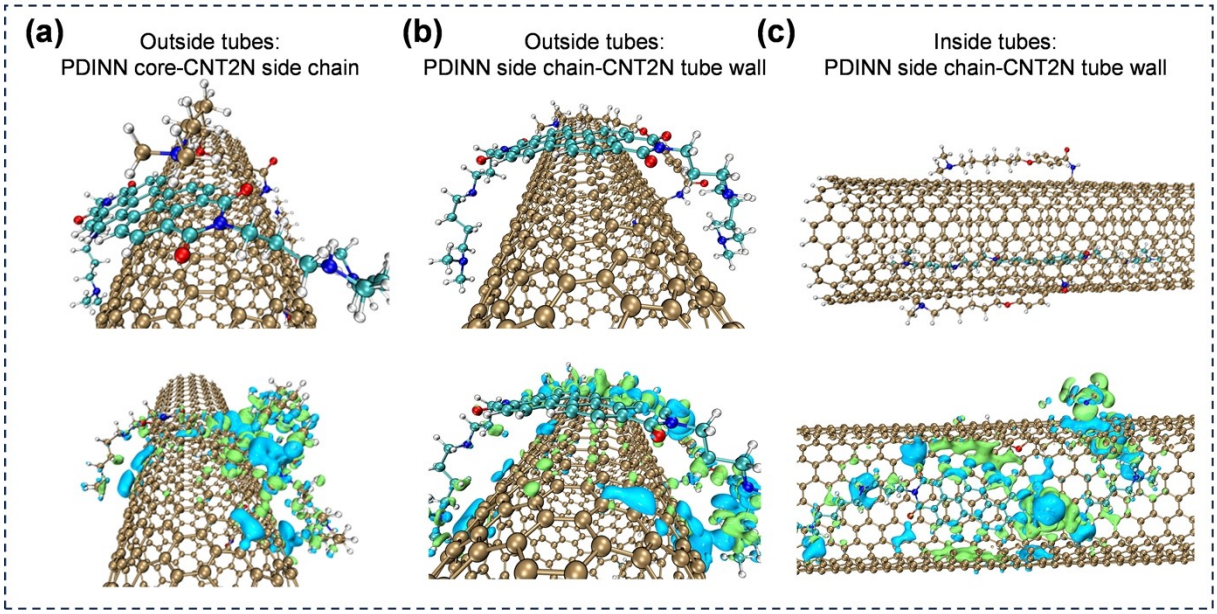

Figure S4. Simulated differential charge density maps of PDINN showing three charge transfer modes outside and inside CNT2N. (a) Charge transfer between the PDINN core and CNT2N side chains. (b) Charge transfer between PDINN side chains and the outer wall of CNT2N. (c) Charge transport between PDINN side chains and the inner wall of CNT2N.

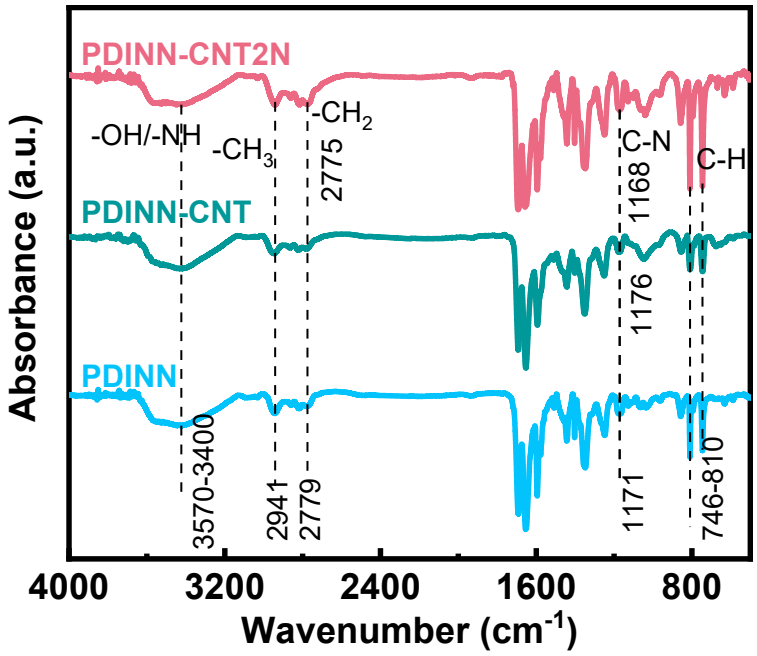

Figure S5. FT-IR spectra of PDINN-CNT2N, PDINN-CNT, and PDINN films.

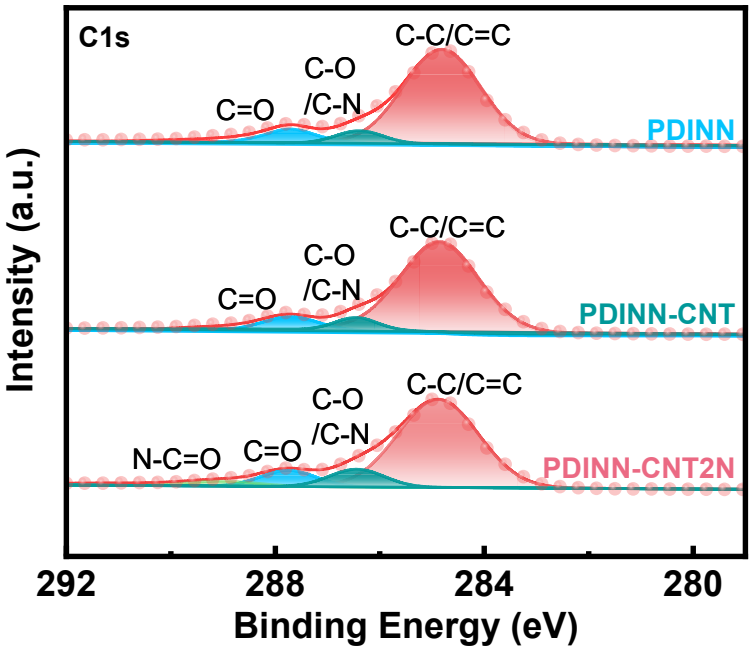

Figure S6. High-resolution XPS spectra of C1s for PDINN, PDINN-CNT and PDINN-CNT2N films.

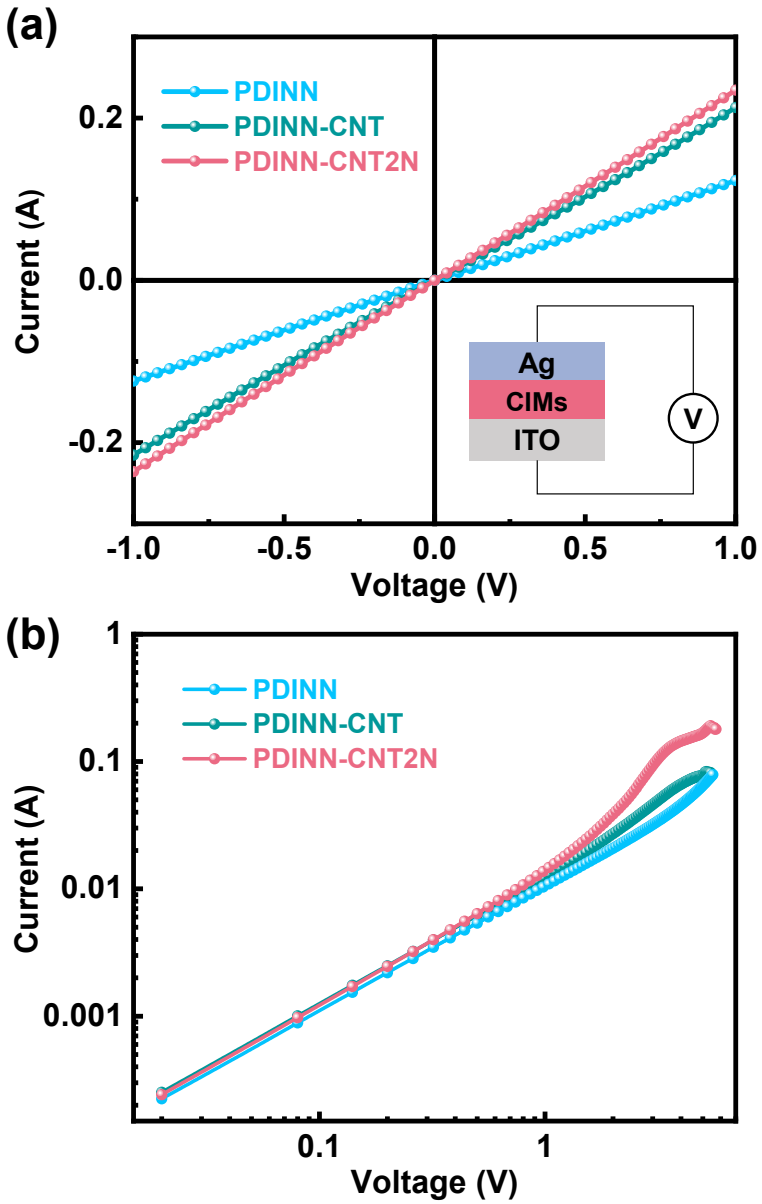

Figure S7. (a) Conductivity and (b) carrier mobility of pristine PDINN, PDINN-CNT, and PDINN-CNT2N CIMs, calculated from the *I-V* characteristics of ITO/CIMs/Ag devices with a CIM thickness of 50 nm.

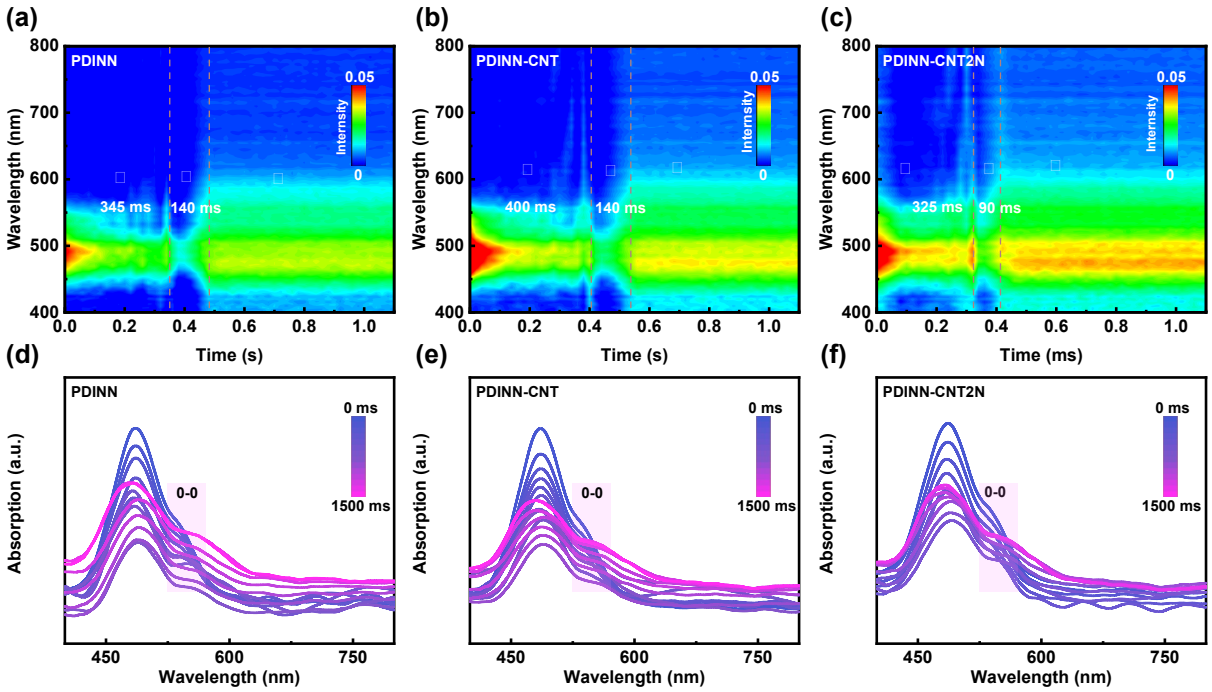

Figure S8. (a-c) 2D time-resolved *in situ* absorption spectra. (d-f) The *in-suit* absoration spectra at the times range from 0~1.5 s of the CIM films based on PDINN, PDINN-CNT, and PDINN-CNT2N.

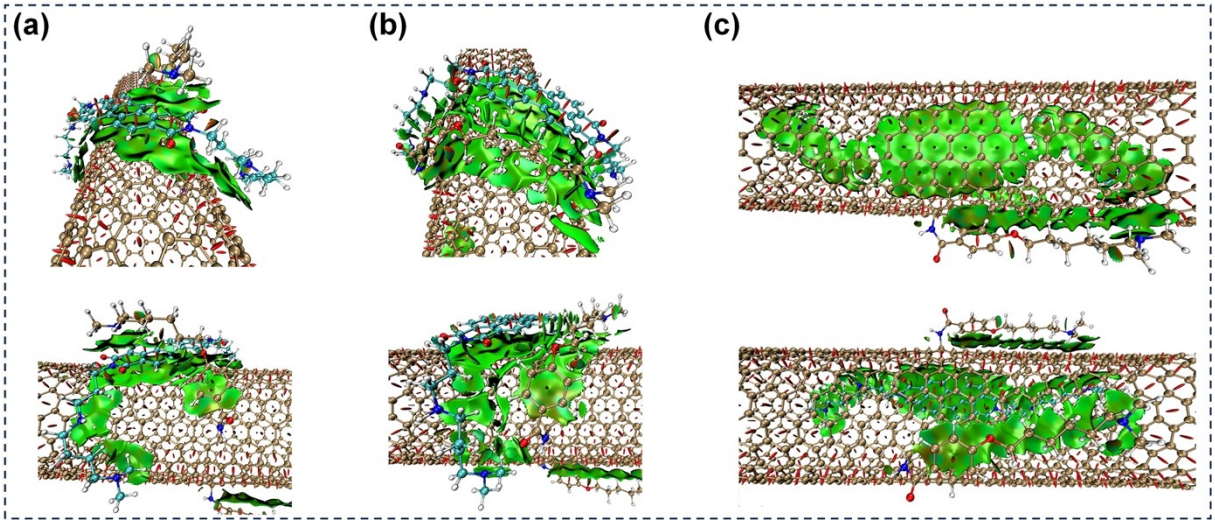

Figure S9. Simulated interaction between PDINN and CNT2N. In all three modes (a-c), π-π stacking interactions were observed on the side-chain interface and tube wall.

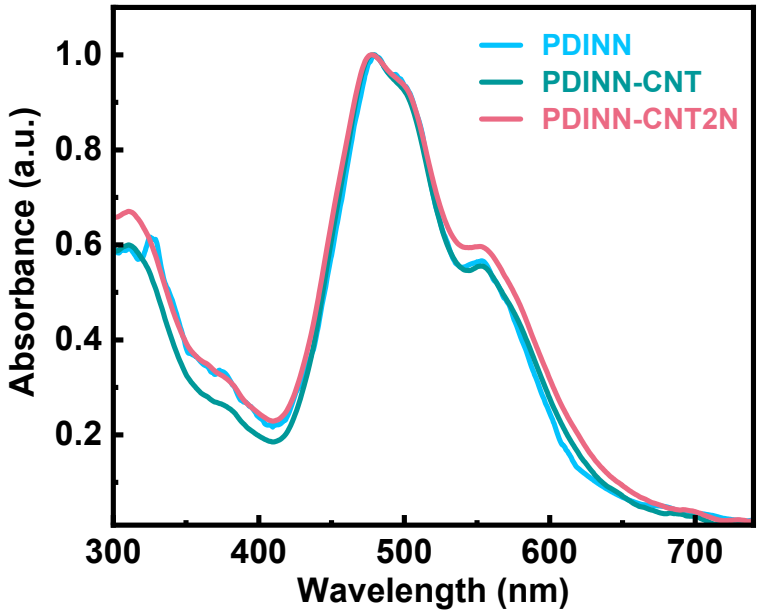

Figure S10. UV-vis absorption spectra for PDINN, PDINN-CNT and PDINN-CNT2N films.

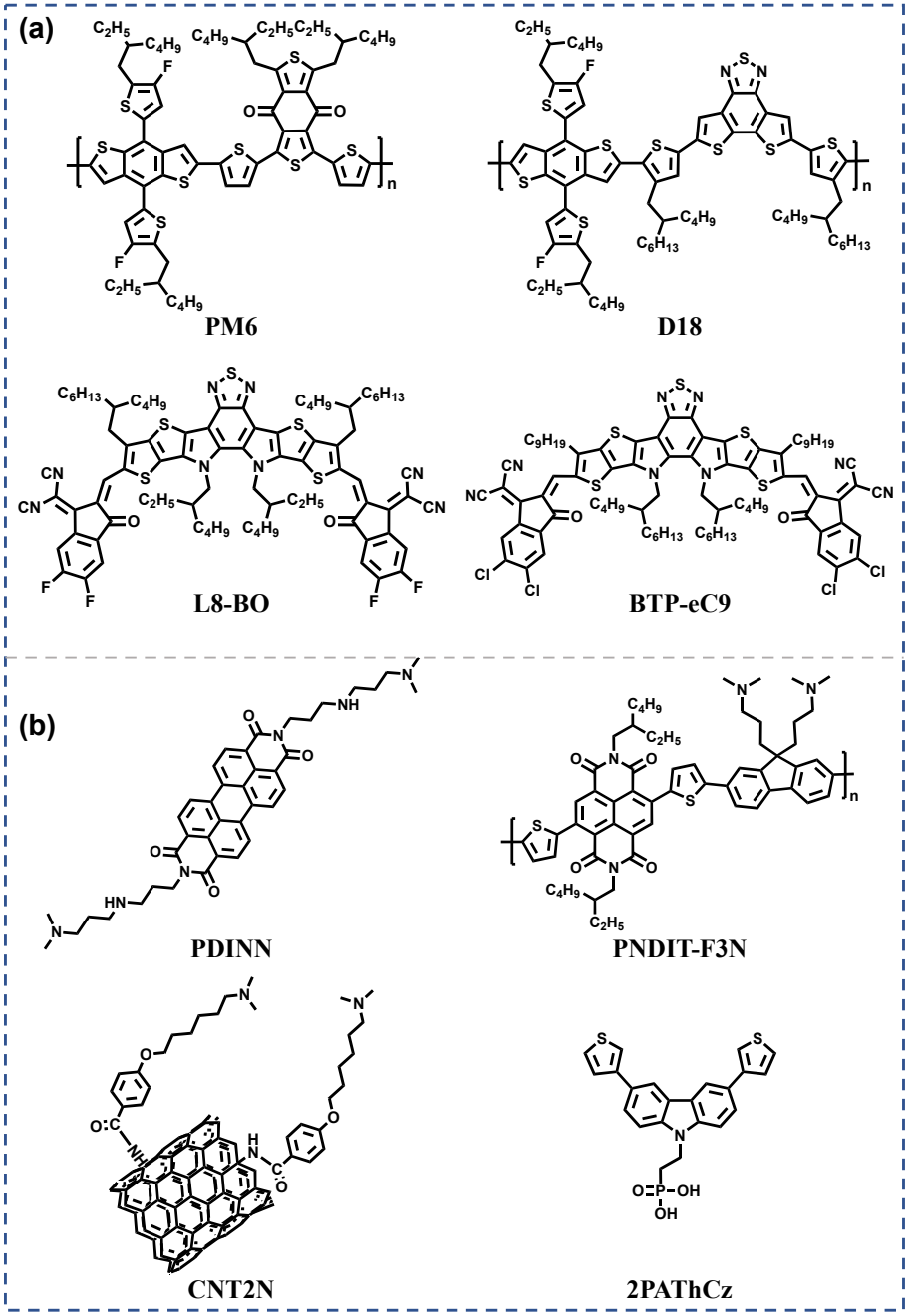

Figure S11. Chemical structures of photoactive and interfacial materials employed in the fabrication of OSCs.

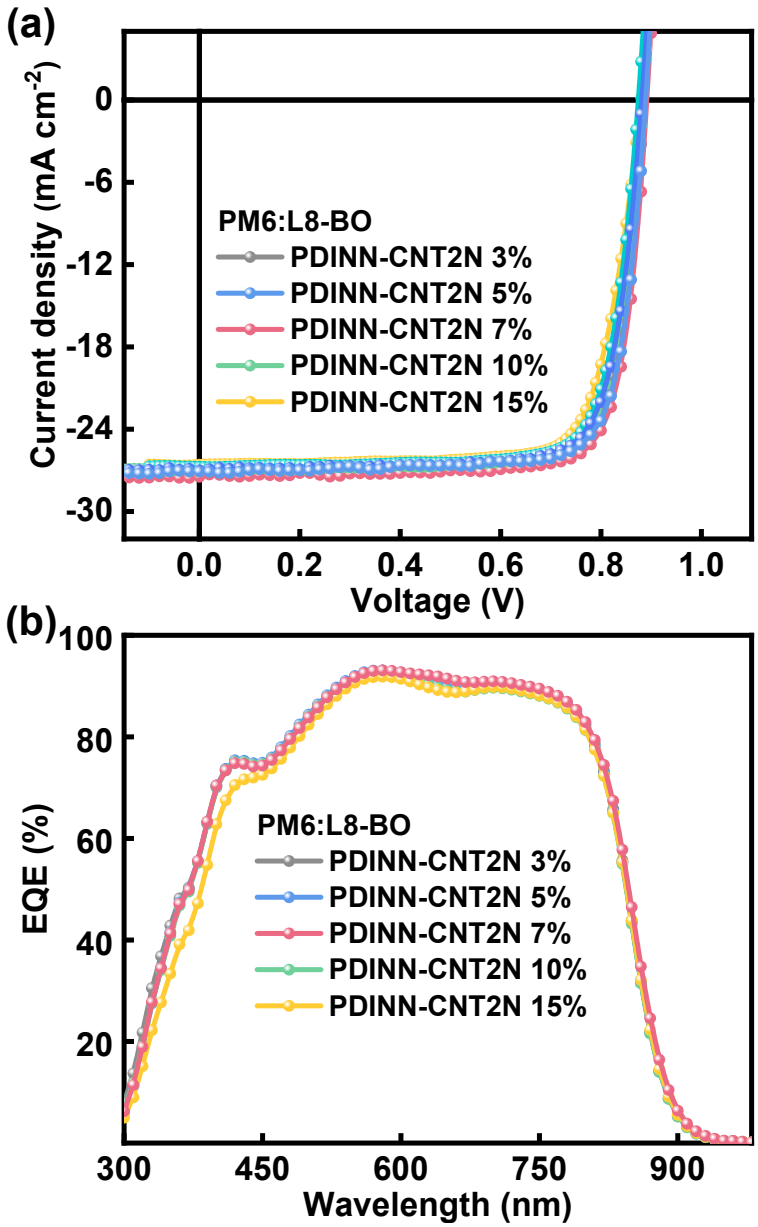

Figure S12. (a) *J-V* curves and (b) corresponding EQE spectra of optimized OSCs based on PM6:L8-BO using PDINN with different doping ratios of CNT2N.

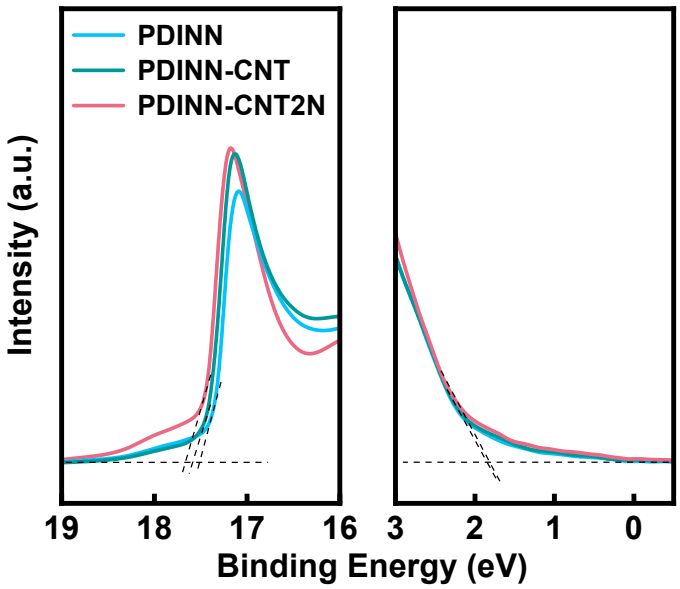

Figure S13. UPS spectra of PDINN-CNT2N, PDINN-CNT, and PDINN films.

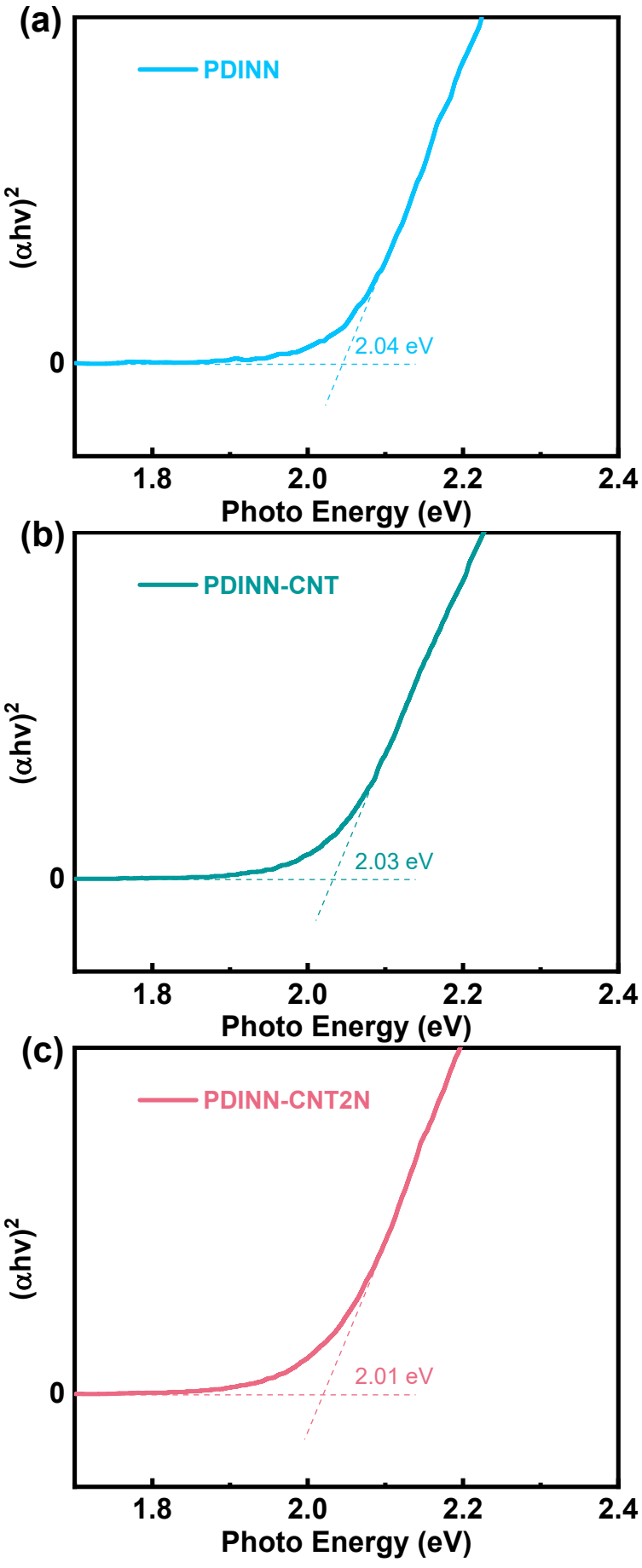

Figure S14. UV-vis spectrum of (a) PDINN, (b) PDINN-CNT, and (c) PDINN-CNT2N films.

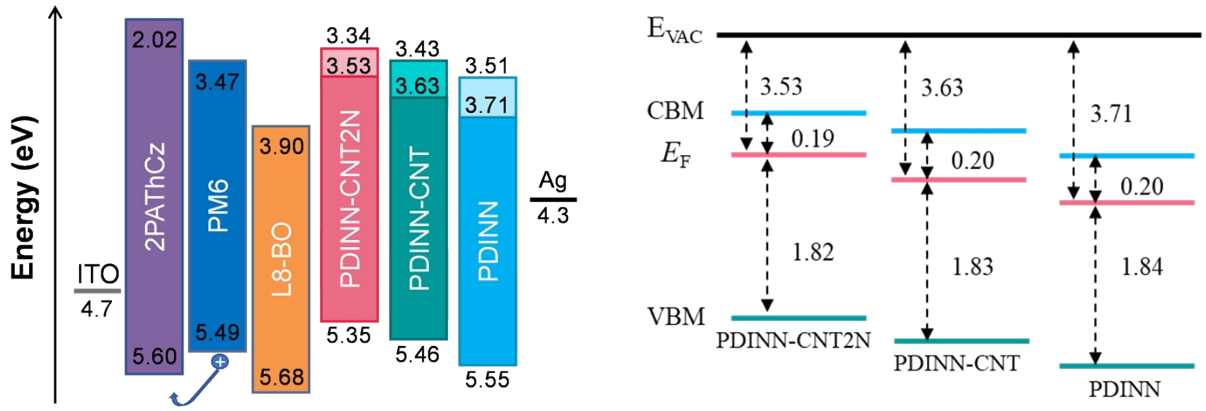

Figure S15. Energy level alignment of the functional layers.

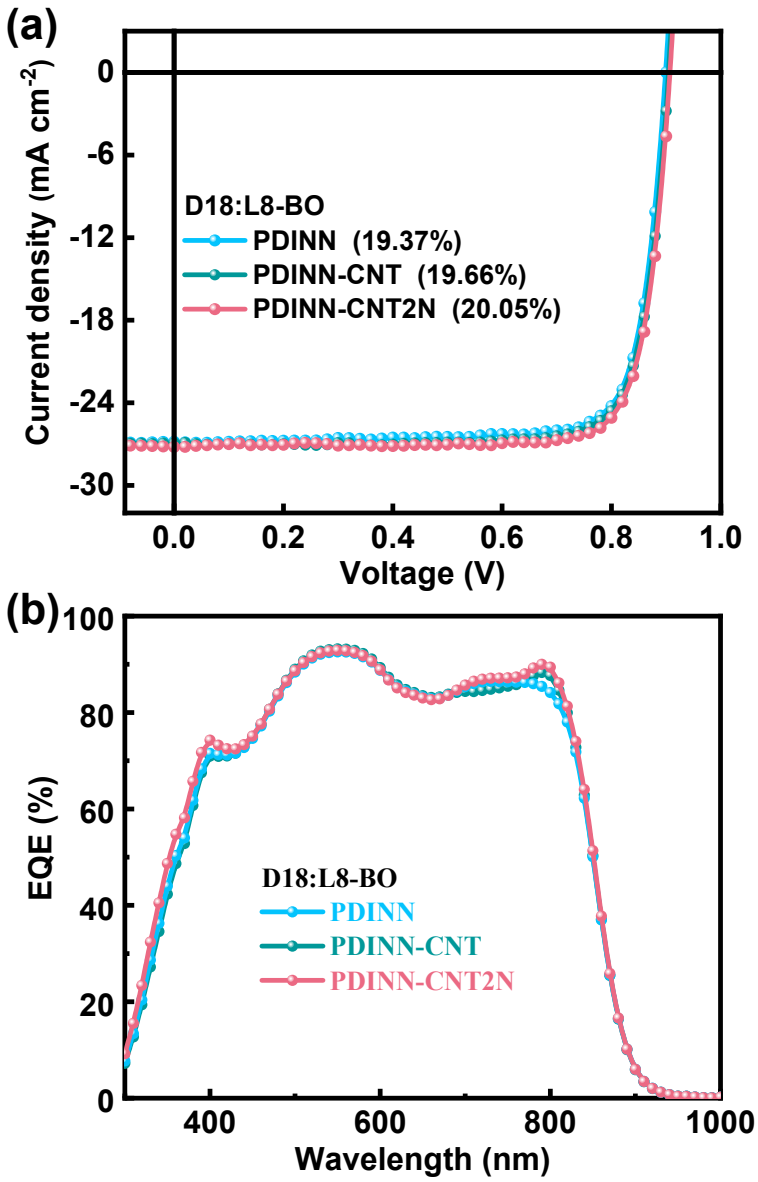

Figure S16. (a) *J-V* curves and (b) corresponding EQE spectra of optimized OSCs based on D18:L8-BO using PDINN-CNT2N, PDINN-CNT, and PDINN CIMs.

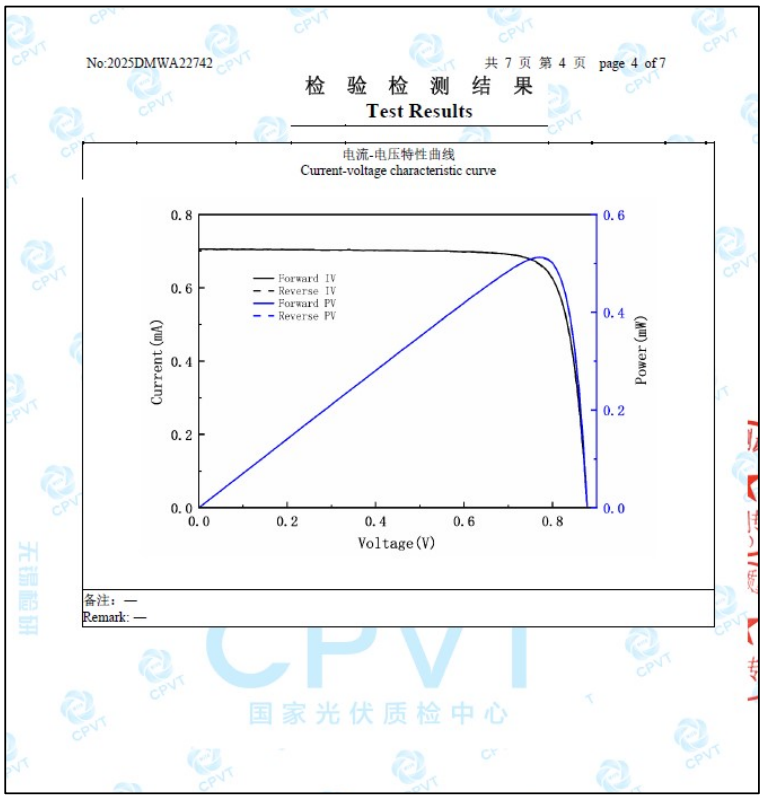

No:2025DMWA22742 共 7 页 第 4 页 page 4 of 7

检 验 检 测 结 果

Test Results

电流-电压特性曲线

Current-voltage characteristic curve

备注：—

Remark: —

No:2025DMWA22742 共 7 页 第 2 页 page 2 of 7

检 验 检 测 结 果

Test Results

序号 Clause	检验项目 Test item(s)	单位 Unit	技术要求 Technical requirements	结果 Results	单项评价 Verdict Pass/Fail
1	电流-电压特性的测量 (正扫) Current-voltage characteristic measurement (Forward scan)	—	在辐照度 1000W/ m² 试验条件下（标准太阳光谱辐照分布符合 IEC 60904-3 规定），测量样品随负荷变化的电流-电压特性。 At irradiance 1000W/m² (standard solar spectral irradiance distribution corresponds to IEC60904-3), measure the current-voltage characteristics of the sample with the variation of load.	—	—
1.1	开路电压 Voc Open-circuit voltage, Voc	V	—	0.8788	—
1.2	短路电流 Isc Short-circuit current, Isc	mA	—	0.7051	—
1.3	最大功率 Pmax Maximum-power, Pmax	mW	—	0.5125	—
1.4	最大功率点电压 Vmp Maximum-power voltage, Vmp	V	—	0.7699	—
1.5	最大功率点电流 Imp Maximum-power current, Imp	mA	—	0.6656	—
1.6	填充因子 FF，% Fill factor FF, %	—	—	82.71	—
1.7	转换效率 η，% Efficiency η, %	—	$\eta = \frac{P_{max}}{1000W/m^2 \times S} \times 100\%$ S 为掩膜板面积/ S denotes the area of the aperture mask	20.33	—

备注：1.测试过程中引入光谱失配修正，光谱失配修正因子为：1.011。

2.正扫扫描方向为-0.1V~1V，步进 0.01V，延迟时间：0s；短路电流密度$J_{sc} = \frac{I_{sc}}{S} = 27.97mA/cm^2$。

计算短路电流密度及转换效率所用面积为掩膜板面积，S = 2.521 mm²。

Remark: 1.The test process takes into account spectra mismatch correction. The spectra mismatch correction factor is 1.011.

2.Forward sweep direction: -0.1V~1V, step: 0.01V, delay time: 0s. $J_{sc} = \frac{I_{sc}}{S} = 277.97mA/cm^2$.

The area used to calculate J_{sc} and efficiency is determined by mask, S = 2.521 mm².

Fig. S17. The certified results from National Center of Inspection on Solar Photovoltaic Products Quality.

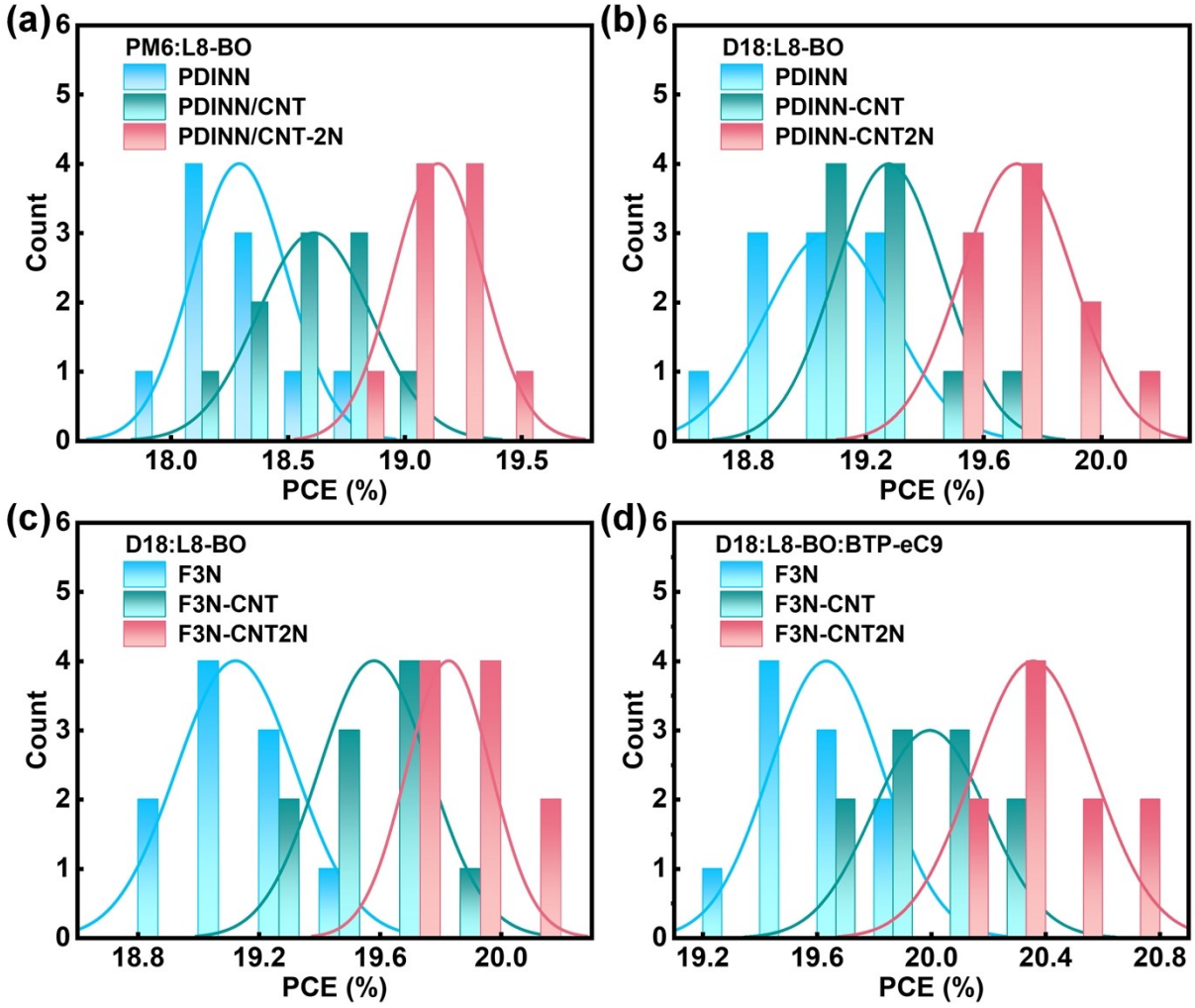

Figure S18. Histogram of the efficiency measurements for OSCs with different CIMs and active layers, fitted with Gaussian distributions (solid lines).

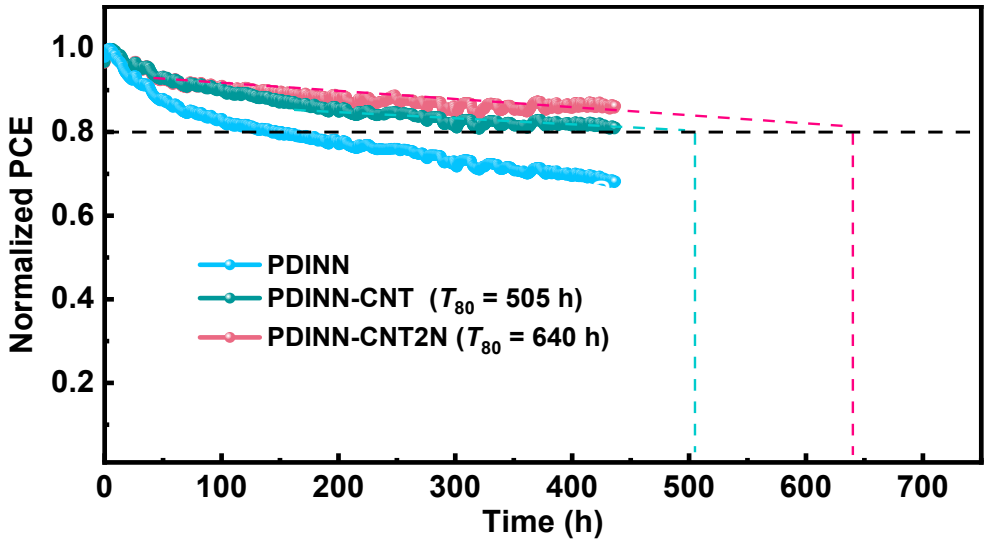

Figure S19. Normalized PCE as a function of aging time under continuous LED illumination for devices fabricated with different CIMs.

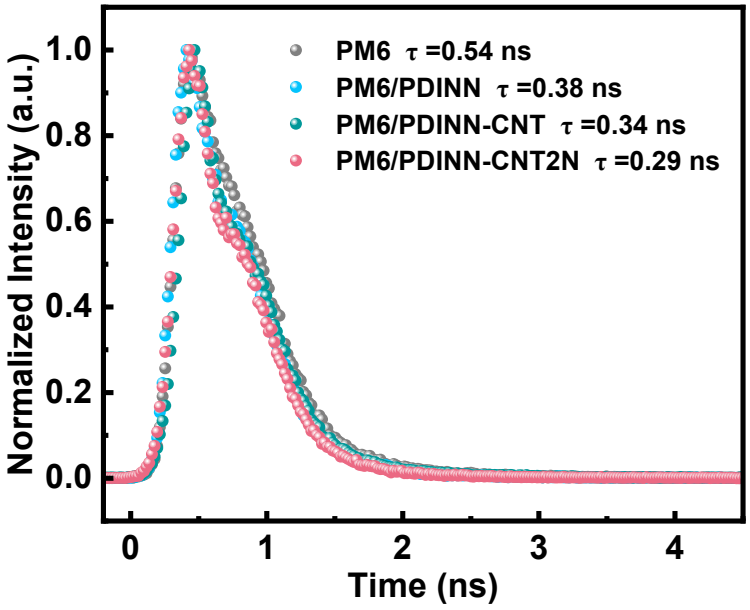

Fig. S20. TRPL spectra of PM6/CIMs bilayer films.

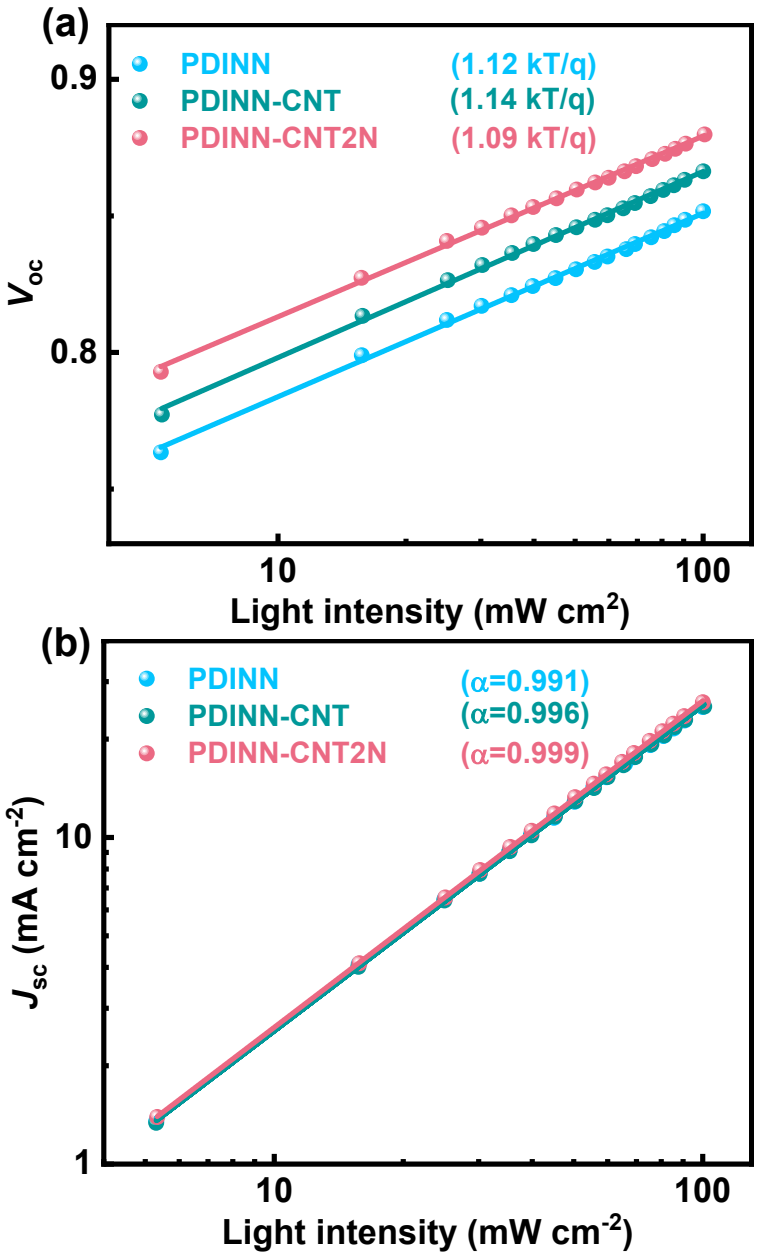

Fig. S21. (a) V_{oc} and (b) J_{sc} versus light intensity of OSC devices processed with different CIMs.

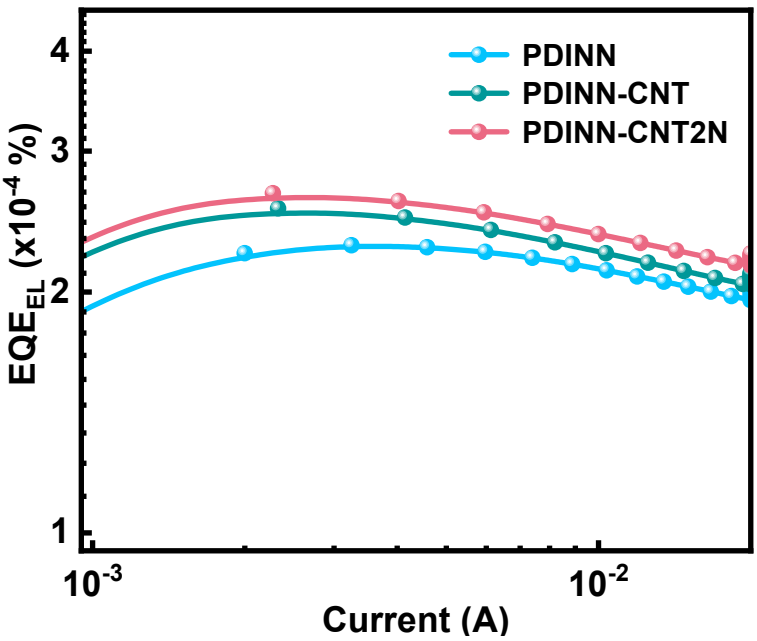

Fig. S22. The EQE_{EL} spectra of OSCs based on PM6:L8-BO using PDINN, PDINN-CNT and PDINN-CNT2N CIMs.

4. Supplementary Tables

Table S1. BE value of C1s, N1s and O1s for different sample involved in this work.

Sample	C1s (eV)				N1s (eV)			O1s (eV)		
	C-C /C=C	C-O/ C-N	C=O	N-C=O	-NH-	C-N	N-O	C=O	C-O-C	C-O
CNT2N	284.8	285.1	287.1	290.1	398.6	400.2	\	533.4	535.5	537.1
CNT	284.8	285.7	290	\	\	400.4	406.3	532.8	\	536.3
Compound S2	284.9	286.3	288.6	\	399.6	401.9	406.7	532.3	533.7	\
PDINN-CNT2N	284.9	286.5	287.8	289.1	398.6	399.6	402.0	531.0	532.7	537
PDINN-CNT	284.9	286.5	287.7	\	399.2	400.1	402.0	531.0	532.7	\
PDINN	284.8	286.4	287.7	\	398.7	399.8	402.0	531.0	532.9	\

Table S2. Differential charge density parameters for the three charge transfer modes based on nitrogen-containing functional groups.

functional groups	Charge density difference (△CHG)		
	Outside tubes		Inside tubes
	side chain-side chain	side chain-tube wall	side chain-tube wall
CNT2N (R_3N)	0.004	0.005	0.003
CNT2N (R_2NH)	0.004	0.003	0.006
PDINN (R_3N)	0.024	0.037	0.012
PDINN (R_2NH)	-0.011	-0.015	0

R_3N and R_2NH denote the tertiary and secondary amine groups, respectively, located on the side chains of PDINN and CNT2N.

Table S3. Calculated measured for GIWAXs data.

CIM	(100) peak along OOP direction			(010) peak along IP direction		
	Location ($Å^{-1}$)	d-spacing (Å)	CCL (Å)	Location ($Å^{-1}$)	d-spacing (Å)	CCL (Å)
PDINN	0.25	25.12	24.77	1.78	3.53	8.79
PDINN-CNT	0.28	22.43	29.56	1.77	3.55	10.57
PDINN-CNT2N	0.28	22.43	36.21	1.78	3.53	11.32

Table S4. Photovoltaic parameters of PM6:L8-BO devices based on different doping ratios of PDINN-CNT2N as CIMs.

CNT2N doping ratio	V_{oc} [V]	J_{sc} [mA cm^{-2}]	J_{EQE}[a] [mA cm^{-2}]	FF [%]	PCE[b] [%]
3%	0.885	27.08	26.12	78.41	18.76 (18.31±0.20)
5%	0.887	27.09	26.17	79.19	19.02 (18.51±0.26)
7%	0.889	27.44	26.59	79.96	19.50 (19.17±0.20)
10%	0.884	26.85	26.03	78.07	18.52 (18.21±0.18)
15%	0.879	26.59	25.74	77.12	18.03 (17.67±0.24)

[a] J_{EQE} was calculated from the EQE spectra. [b] Average PCEs with standard deviations were calculated from 10 individual devices.

Table S5. Summary of energy level parameters for three different interfacial transport layers.

CIMs	E_{cutoff} [eV]	E_g [eV]	WF [eV]	E_{VB} [eV]	VBM [eV]	E_{CB} [eV]	CBM [eV]
PDINN	17.51	2.04	3.71	1.84	5.55	0.20	3.51
PDINN-CNT	17.59	2.03	3.63	1.83	5.46	0.20	3.43
PDINN-CNT2N	17.69	2.01	3.53	1.82	5.35	0.19	3.34

E_{CB} denotes the energy difference between the conduction band minimum (CBM) and the Fermi level (E_F); E_{VB} denotes the energy difference between the valence band maximum (VBM) and E_F.

Table S6. Photovoltaic parameters of 10 individual PM6:L8-BO devices based on PDINN CIM without CNT2N.

CIM	Active layer	V_{oc} [V]	J_{sc} [mA cm^{-2}]	*FF* [%]	PCE [%]
PDINN-CNT2N 0%	PM6:L8-BO	0.884	26.61	79.55	18.71
		0.880	26.93	78.42	18.57
		0.881	26.98	77.69	18.43
		0.875	26.82	78.06	18.31
		0.883	26.65	77.66	18.28
		0.870	26.57	78.80	18.22
		0.886	25.98	78.89	18.15
		0.886	26.88	76.11	18.12
		0.872	26.70	77.85	18.11
		0.883	26.21	78.03	18.06
Average		0.880±0.006	26.63±0.32	78.11±0.92	18.29±0.20

Table S7. Photovoltaic parameters of 10 individual PM6:L8-BO devices based on PDINN-CNT2N with a CNT2N doping mass ratio of 3%.

CIM	Active layer	V_{oc} [V]	J_{sc} [mA cm^{-2}]	*FF* [%]	PCE [%]
PDINN-CNT2N 3%	PM6:L8-BO	0.885	27.08	78.41	18.76
		0.878	27.29	77.27	18.49
		0.878	27.11	77.44	18.4
		0.885	26.09	79.52	18.36
		0.881	26.48	78.41	18.27
		0.881	26.13	79.25	18.23
		0.885	25.93	79.27	18.19
		0.880	26.07	79.06	18.14
		0.881	26.2	78.59	18.13
		0.885	26.2	78.32	18.13
Average		0.882±0.003	26.46±0.51	78.55±0.76	18.31±0.20

Table S8. Photovoltaic parameters of 10 individual PM6:L8-BO devices based on PDINN-CNT2N CIM with a CNT2N doping mass ratio of 5%.

CIM	Active layer	V_{oc} [V]	J_{sc} [mA cm^{-2}]	*FF* [%]	PCE [%]
PDINN-CNT2N 5%	PM6:L8-BO	0.887	27.09	79.19	19.02
		0.888	26.84	78.70	18.75
		0.878	26.87	79.47	18.74
		0.877	26.73	79.39	18.61
		0.884	26.94	77.65	18.46
		0.88	26.73	78.31	18.42
		0.876	26.81	78.00	18.32
		0.88	26.66	77.97	18.3
		0.877	27.41	76.04	18.28
		0.883	26.67	77.43	18.24
Average		0.881±0.004	26.88±0.23	78.22±1.05	18.51±0.26

Table S9. Photovoltaic parameters of 10 individual PM6:L8-BO devices based on PDINN-CNT2N CIM with a CNT2N doping mass ratio of 7%.

CIM	Active layer	V_{oc} [V]	J_{sc} [mA cm^{-2}]	*FF* [%]	PCE [%]
PDINN-CNT2N 7%	PM6:L8-BO	0.889	27.44	79.96	19.50
		0.886	27.31	78.90	19.33
		0.878	27.58	79.80	19.31
		0.891	27.14	79.62	19.24
		0.873	27.61	79.50	19.16
		0.879	27.55	78.87	19.08
		0.881	27.48	78.70	19.04
		0.887	27.15	79.06	19.03
		0.888	27.31	78.02	18.92
		0.893	27.14	77.83	18.84
Average		0.885±0.006	27.37±0.19	79.03±0.72	19.17±0.20

Table S10. Photovoltaic parameters of 10 individual PM6:L8-BO devices based on PDINN-CNT2N CIM with a CNT2N doping mass ratio of 10%.

CIM	Active layer	V_{oc} [V]	J_{sc} [mA cm^{-2}]	*FF* [%]	PCE [%]
PDINN-CNT2N 10%	PM6:L8-BO	0.884	26.85	78.07	18.52
		0.882	26.35	79.23	18.41
		0.883	26.4	78.67	18.33
		0.886	26.5	77.76	18.24
		0.882	26.47	78.29	18.27
		0.878	26.07	79.18	18.13
		0.882	26.51	77.54	18.12
		0.877	26.35	77.98	18.03
		0.880	25.79	79.29	18.00
		0.870	26.98	76.76	17.99
Average		0.880±0.004	26.43±0.34	78.28±0.83	18.21±0.18

Table S11. Photovoltaic parameters of 10 individual PM6:L8-BO devices based on PDINN-CNT2N CIM with a CNT2N doping mass ratio of 15%.

CIM	Active layer	V_{oc} [V]	J_{sc} [mA cm^{-2}]	*FF* [%]	PCE [%]
PDINN-CNT2N 15%	PM6:L8-BO	0.879	26.59	77.12	18.03
		0.878	26.55	77.20	18.01
		0.877	26.42	76.87	17.81
		0.870	26.45	77.30	17.79
		0.872	26.42	76.67	17.66
		0.870	26.42	76.71	17.63
		0.861	26.49	76.88	17.54
		0.867	26.24	76.76	17.46
		0.864	26.51	76.01	17.41
		0.867	26.41	75.71	17.34
Average		0.871±0.006	26.45±0.10	76.72±0.51	17.68±0.24

Table S12. Photovoltaic parameters of 10 individual PM6:L8-BO devices based on PDINN-CNT CIM with a CNT doping mass ratio of 7%.

CIM	Active layer	V_{oc} [V]	J_{sc} [mA cm^{-2}]	*FF* [%]	PCE [%]
PDINN-CNT 7%	PM6:L8-BO	0.885	27.06	79.67	19.08
		0.887	26.90	79.12	18.85
		0.882	26.95	79.25	18.81
		0.887	26.90	78.47	18.72
		0.875	26.86	79.19	18.61
		0.880	27.43	76.95	18.55
		0.883	26.31	79.68	18.51
		0.881	26.35	79.50	18.46
		0.881	26.32	79.26	18.37
		0.881	26.44	78.90	18.38
Average		0.882±0.004	26.75±0.38	78.99±0.80	18.63±0.23

Table S13. Photovoltaic parameters of 10 individual D18:L8-BO devices based on PDINN CIM without CNT2N.

CIM	Active layer	V_{oc} [V]	J_{sc} [mA cm^{-2}]	*FF* [%]	PCE [%]
PDINN-CNT2N 0%	D18:L8-BO	0.897	26.85	80.43	19.37
		0.896	26.81	80.40	19.31
		0.896	26.90	80.13	19.29
		0.900	26.84	79.22	19.13
		0.901	26.38	80.33	19.09
		0.900	26.82	78.99	19.08
		0.896	26.72	79.27	18.98
		0.892	26.78	79.21	18.92
		0.900	26.25	79.80	18.85
		0.899	26.24	79.33	18.70
Average		0.897±0.003	26.70±0.20	79.83±0.65	19.11±0.17

Table S14. Photovoltaic parameters of 10 individual D18:L8-BO devices based on PDINN-CNT CIM with a CNT doping mass ratio of 7%.

CIM	Active layer	V_{oc} [V]	J_{sc} [mA cm^{-2}]	*FF* [%]	PCE [%]
PDINN-CNT 7%	D18:L8-BO	0.902	26.91	80.98	19.66
		0.901	26.64	81.03	19.45
		0.902	26.73	80.35	19.38
		0.900	26.73	80.39	19.35
		0.899	26.46	80.80	19.23
		0.900	26.82	79.57	19.22
		0.904	26.57	79.84	19.18
		0.901	26.33	80.78	19.16
		0.902	26.51	79.76	19.08
		0.899	26.25	80.77	19.07
Average		0.901±0.002	26.60±0.21	80.43±0.54	19.28±0.18

Table S15. Photovoltaic parameters of 10 individual D18:L8-BO devices based on PDINN-CNT2N CIM with a CNT2N doping mass ratio of 7%.

CIM	Active layer	V_{oc} [V]	J_{sc} [mA cm^{-2}]	*FF* [%]	PCE [%]
PDINN-CNT2N 7%	D18:L8-BO	0.905	27.19	81.46	20.05
		0.904	27.09	81.29	19.91
		0.901	26.97	81.73	19.86
		0.901	27.05	81.16	19.78
		0.905	26.75	81.56	19.73
		0.897	27.07	80.78	19.62
		0.902	26.86	80.91	19.61
		0.901	26.84	80.98	19.58
		0.900	26.68	81.43	19.56
		0.900	26.85	80.38	19.43
Average		0.902±0.002	26.94±0.16	81.17±0.41	19.71±0.19

Table S16. Photovoltaic parameters of 10 individual D18:L8-BO devices based on F3N CIM without CNT2N.

CIM	Active layer	V_{oc} [V]	J_{sc} [mA cm^{-2}]	*FF* [%]	PCE [%]
F3N-CNT2N 0%	D18:L8-BO	0.904	26.82	80.47	19.51
		0.905	26.48	80.51	19.29
		0.902	26.81	79.74	19.28
		0.903	26.69	79.80	19.23
		0.901	26.40	80.28	19.09
		0.902	26.29	80.10	18.98
		0.898	26.55	79.51	18.96
		0.899	26.62	79.17	18.96
		0.902	26.50	79.02	18.90
		0.889	27.10	78.21	18.85
Average		0.901±0.005	26.63±0.24	79.68±0.73	19.11±0.21

Table S17. Photovoltaic parameters of 10 individual D18:L8-BO devices based on F3N-CNT CIM with a CNT doping mass ratio of 7%.

CIM	Active layer	V_{oc} [V]	J_{sc} [mA cm^{-2}]	*FF* [%]	PCE [%]
F3N-CNT 7%	D18:L8-BO	0.905	26.88	81.38	19.80
		0.909	26.62	81.73	19.78
		0.907	26.73	81.57	19.78
		0.905	26.77	81.44	19.73
		0.906	26.68	81.52	19.71
		0.903	27.01	80.44	19.62
		0.905	26.47	81.54	19.53
		0.907	26.58	80.86	19.49
		0.901	26.45	81.08	19.32
		0.902	26.88	79.44	19.25
Average		0.905±0.003	26.71±0.18	81.1±0.70	19.60±0.20

Table S18. Photovoltaic parameters of 10 individual D18:L8-BO devices based on F3N-CNT2N CIM with a CNT2N doping mass ratio of 7%.

CIM	Active layer	V_{oc} [V]	J_{sc} [mA cm^{-2}]	*FF* [%]	PCE [%]
F3N-CNT2N 7%	D18:L8-BO	0.911	26.90	81.88	20.08
		0.912	26.78	81.91	20.01
		0.907	26.85	81.75	19.91
		0.913	26.74	81.43	19.87
		0.911	26.45	82.47	19.86
		0.907	26.84	81.46	19.83
		0.902	26.77	81.72	19.73
		0.903	26.82	81.29	19.70
		0.906	26.63	81.50	19.66
		0.904	26.47	82.09	19.64
Average		0.907±0.004	26.73±0.16	81.75±0.35	19.83±0.15

Table S19. Photovoltaic parameters of 10 individual D18:L8-BO:BTP-eC9 devices based on F3N CIM without CNT2N.

CIM	Active layer	V_{oc} [V]	J_{sc} [mA cm^{-2}]	*FF* [%]	PCE [%]
F3N-CNT2N 0%	D18:L8-BO:BTP-eC9	0.882	28.14	80.32	19.93
		0.880	27.99	80.65	19.87
		0.881	28.28	79.66	19.85
		0.877	27.99	80.76	19.82
		0.884	28.00	79.60	19.70
		0.887	28.08	78.65	19.58
		0.879	28.01	79.36	19.53
		0.882	27.53	80.43	19.52
		0.879	27.92	79.12	19.42
		0.878	27.66	79.55	19.30
Average		0.881±0.003	27.95±0.22	79.81±0.70	19.65±0.21

Table S20. Photovoltaic parameters of 10 individual D18:L8-BO:BTP-eC9 devices based on F3N-CNT CIM with a CNT doping mass ratio of 7%.

CIM	Active layer	V_{oc} [V]	J_{sc} [mA cm^{-2}]	*FF* [%]	PCE [%]
F3N-CNT 7%	D18:L8-BO:BTP-eC9	0.884	28.21	81.16	20.24
		0.883	28.26	81.00	20.21
		0.881	28.48	80.45	20.17
		0.883	27.96	81.63	20.13
		0.879	28.27	80.61	20.02
		0.880	28.16	80.71	19.99
		0.880	28.30	80.09	19.92
		0.884	27.83	80.61	19.84
		0.881	27.85	80.69	19.79
		0.881	28.19	79.09	19.63
Average		0.882±0.002	28.15±0.21	80.61±0.68	19.99±0.20

Table S21. Photovoltaic parameters of 10 individual D18:L8-BO:BTP-eC9 devices based on F3N-CNT2N CIM with a CNT2N doping mass ratio of 7%.

CIM	Active layer	V_{oc} [V]	J_{sc} [mA cm^{-2}]	*FF* [%]	PCE [%]
F3N-CNT2N 7%	D18:L8-BO:BTP-eC9	0.888	28.55	81.72	20.72
		0.887	28.60	81.29	20.61
		0.881	28.63	80.94	20.41
		0.880	28.60	80.99	20.38
		0.888	28.38	80.45	20.27
		0.877	28.55	80.76	20.22
		0.891	28.15	80.36	20.16
		0.885	28.10	81.00	20.14
		0.887	28.08	80.81	20.13
		0.881	28.28	80.70	20.11
Average		0.885±0.004	28.39±0.22	80.90±0.40	20.32±0.21

Table S22. Summary of PCEs for binary OSCs reported in the literature.

Reference	CIMs	PCE	No.
Nat. Energy, 2021, **6**, 605	PNDIT-F3N-Br	18.32	B1
Matter, 2021, **4**, 2542	PNDIT-F3N	18.60	B2
Angew. Chem. Int. Ed., 2021, **133**, 22728	PNDIT-F3N	18.77	B3
Energy Environ. Sci., 2022, **15**, 2537	Bis-FIMG	18.5	B4
Adv. Sci., 2022, **9**, 2200578	PNDIT-F3N	18.7	B5
Adv. Mater., 2022, **34**, 2204718	PDIN	19.05	B6
Adv. Mater., 2022, **34**, 2203379	PFN-Br	18.86	B7
Adv. Energy Mater., 2023, **13**, 2203009	PDINN	19.0	B8
Adv. Mater., 2023, **35**, 2208211	PDINN	19.0	B9
Adv. Mater., 2023, **35**, 2211871	PNDIT-F3N	19.02	B10
Energy Environ. Sci., 2023, **16**, 3441	PNDI-F3N-Br	19.1	B11
Angew. Chem. Int. Ed., 2023, **62**, e202309713	PDINO	18.85	B12
Nat. Commun., 2023, **14**, 6964	PNDIT-F3N	19.04	B13
Angew. Chem. Int. Ed., 2023, **62**, e202314420	PNDIT-F3N	19.65	B14
Adv. Funct. Mater., 2024, **34**, 2309832	PDIN	18.9	B15
Small, 2024, **20**, 2308165	PDINN	19.1	B16
Adv. Mater., 2024, **36**, 2308608	PDINN	19.2	B17
Adv. Funct. Mater., 2024, **34**, 2401823	PDINN	19.07	B18
Nat. Energy, 2021, **9**, 208	PDINN	19.1	B19
Adv. Mater., 2024, **36**, 2312635	GDY-N	19.30	B20
Angew. Chem. Int. Ed., 2024, **63**, e202316227	PDINN	19.3	B21
Energy Environ. Sci., 2024, **17**, 1916	PDINN	19.1	B22
Joule, 2024, **8**, 835	PDINN	19.7	B23
Angew. Chem. Int. Ed., 2025, **64**, e202421953	PDINN	19.51	B24
Nat. Mater., 2025, **24**, 433	PNDIT-F3N	19.78	B25
/	PDINN-CNT2N	20.05	This work
/	PDINN-CNT2N	20.08	This work

Table S23. Summary of PCEs for ternary OSCs reported in the literature.

Reference DOI	CIMs	PCE	Number
Adv. Mater., 2021, **33**, 2101733	PNDIT-F3N	18.66	T1
Energy Environ. Sci., 2022, **15**, 2537	Bis-FIMG	19.2	T2
Adv. Mater., 2022, **34**, 2110147	PNDIT-F3N	19.17	T3
Adv. Mater., 2022, **35**, 2208750	PNDIT-F3NBr	19.12	T4
Small, 2023, **19**, 2207505	BCP	19.33	T5
Adv. Mater., 2023, **35**, 2208997	PNDIT-F3N	19.61	T6
Adv. Sci., 2023, **10**, 2206580	PNDIT-F3N	19.1	T7
Adv. Mater., 2023, **35**, 2300631	PNDIT-F3N	19.54	T8
Adv. Energy Mater., 2023, **13**, 2300763	PNDIT-F3NBr	19.1	T9
Adv. Funct. Mater., 2023, **33**, 2305765	PDINN	19.1	T10
Angew. Chem. Int. Ed., 2023, **135**, e202308307	PFN-Br-MA	19.23	T11
Energy Environ. Sci., 2023, **16**, 2316	PFN-Br-MA	19.1	T12
Nat. Commun., 2023, **14**, 6297	PDINN	19.4	T13
Adv. Mater., 2023, **35**, 2304921	PDINN	19.3	T14
Energy Environ. Sci., 2023, **16**, 5944	PNDIT-F3N	19.01	T15
Angew. Chem. Int. Ed., 2024, **136**, e202316295	PNDIT-F3N	19.31	T16
Adv. Funct. Mater., 2024, **34**, 2311512	PNDIT-F3N	19.43	T17
J. Am. Chem. Soc., 2024, **146**, 14287	PNDIT-F3N	19.71	T18
Adv. Mater., 2024, **36**, 2400342	PDINN	20.17	T19
Nat. Energy, 2024, **9**, 975	PDINN	20.20	T20
Sci. China Chem., 2024, **67**, 1	NDI-PhC4	20.20	T21
Angew. Chem. Int. Ed., 2025, **64**, e202423562.	PNDIT-F3N	20	T22
Nat. Mater., 2025, **24**, 433	PNDIT-F3N	20.42	T23
J. Am. Chem. Soc., 2025, **147**, 4631	PFN-Br	19.82	T24
Energy Environ. Sci., 2025, **18**, 2298.	PDINN	20.2	T25
/	F3N-CNT2N	20.72	This work

Table S24. Summary of device characterization parameters based on different CIMs.

CIMs	V_{bi} [V]	R_s [KΩ]	J_{sat} [mA cm^{-2}]	J_{sc} [mA cm^{-2}]	J_{ph} [mA cm^{-2}]	J_{sc}/J_{sat} [%]	J_{ph}/J_{sat} [%]	μ_e [10^{-5} cm^2 V^{-1} s^{-1}]
PDINN	0.593	10.64	27.15	26.93	24.47	99.18	90.13	2.68
PDINN-CNT	0.609	1.12	27.21	26.74	24.60	98.27	90.41	2.96
PDINN-CNT2N	0.637	0.71	27.63	27.43	25.42	99.28	92.00	10.4

J_{ph} at the maximizing power output voltage.

5. NMR of the compounds

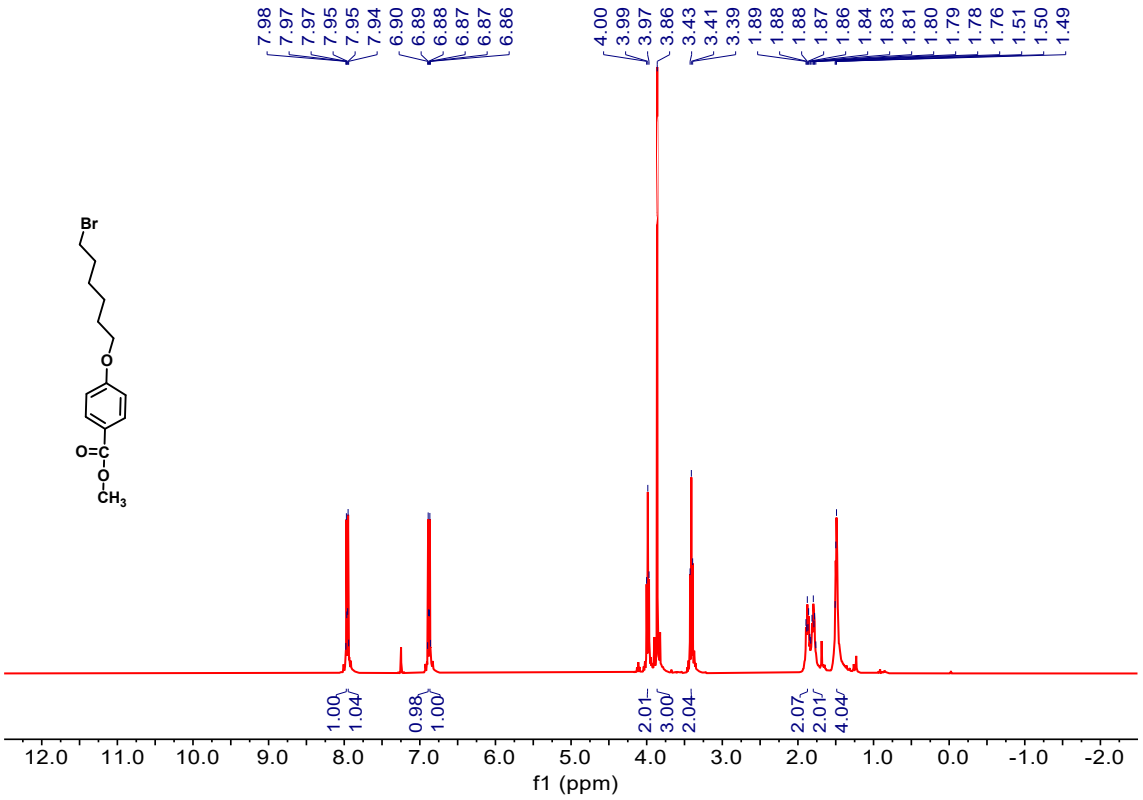

Figure S18. ^{1}H-NMR of the compound S1 recorded in $CDCl_3$.

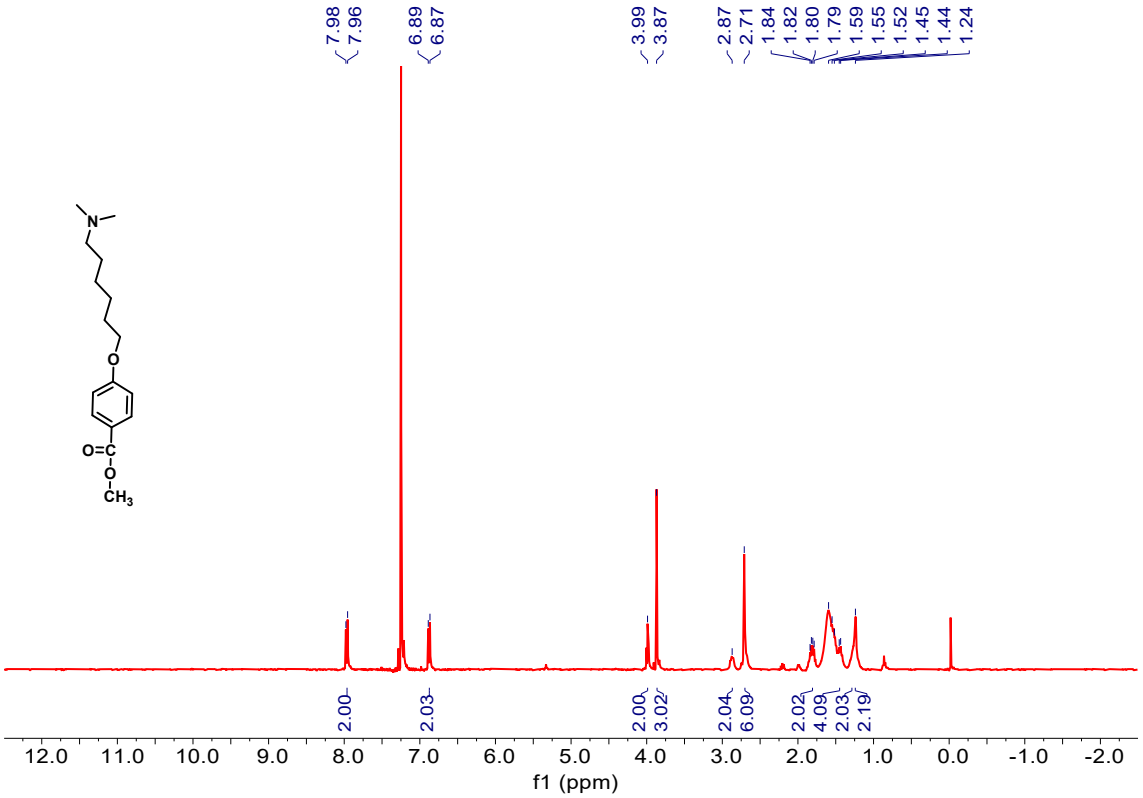

Figure S19. ^{1}H-NMR of the compound S2 recorded in $CDCl_3$.

6. References

1. B. V. Basheer, J. J. George, S. Siengchin and J. Parameswaranpillai, *Nano-Structures & Nano-Objects*, **2020**, *22*, 100429.
2. Y. Xie, J. Tian, X. Yang, J. Chen, S. Yu, D. Tang, X. Hu, Y. Sun and M. Lv, *Adv. Mater.*, **2025**, e02485, DOI: 10.1002/adma.202502485.
3. F. Pan, C. Sun, Y. Li, D. Tang, Y. Zou, X. Li, S. Bai, X. Wei, M. Lv, X. Chen and Y. Li, *Energy & Environmental Science*, **2019**, *12*, 3400-3411.
4. F. Pan, S. Bai, X. Wei, Y. Li, D. Tang, X. Chen, M. Lv and Y. Li, *Science China Materials*, **2020**, *64*, 277-287.
5. L. Liu, Y. Kan, K. Gao, J. Wang, M. Zhao, H. Chen, C. Zhao, T. Jiu, A. K. Y. Jen and Y. Li, *Adv. Mater.*, **2020**, *32*, 1907604.
6. L. Yang, S. Shen, X. Chen, H. Wei, D. Xia, C. Zhao, N. Zhang, Y. Hu, W. Li, H. Xin and J. Song, *Adv. Funct. Mater.*, **2023**, *33*, 2303603.
7. C. Xie, C. Xiao, J. Fang, C. Zhao and W. Li, *Nano Energy*, **2023**, *107*, 108153.
8. Y. Wang, J. Wen, Z. Shang, Y. Zhong, H. Zhang, W. Liu, W. Han, H. Yang, J. Liu, J. Zhang, H. Li and Y. Liu, *Angew. Chem. Int. Ed.*, **2025**, *137*, e202506252.